HAL
open science

Synthesis of a double-stranded spiroborate helicate bearing stilbene units and its photoresponsive behaviour

Daisuke Taura, Heejun Min, Claudine Katan, Eiji Yashima

To cite this version:

Daisuke Taura, Heejun Min, Claudine Katan, Eiji Yashima. Synthesis of a double-stranded spiroborate helicate bearing stilbene units and its photoresponsive behaviour. New Journal of Chemistry, 2014, 39 (5), pp.3259-3269. 10.1039/C4NJ01669F . hal-01081618

HAL Id: hal-01081618

https://univ-rennes.hal.science/hal-01081618v1

Submitted on 10 Nov 2014

HAL is a multi-disciplinary open access archive for the deposit and dissemination of scientific research documents, whether they are published or not. The documents may come from teaching and research institutions in France or abroad, or from public or private research centers.

L'archive ouverte pluridisciplinaire **HAL**, est destinée au dépôt et à la diffusion de documents scientifiques de niveau recherche, publiés ou non, émanant des établissements d'enseignement et de recherche français ou étrangers, des laboratoires publics ou privés.

Copyright

Synthesis of a double-stranded spiroborate helicate bearing stilbene units and its photoresponsive behaviour†

Daisuke Taura,[a] Heejun Min,[a] Claudine Katan[b] and Eiji Yashima*[a]

Received (in XXX, XXX) Xth XXXXXXXXX 20XX, Accepted Xth XXXXXXXXX 20XX
DOI: 10.1039/b000000x

A novel spiroborate-based double-stranded helicate bearing photoresponsive *cis*-stilbene units in the middle (*cis*-**3**) was successfully synthesised from the corresponding *cis*-stilbene-bound tetraphenol strand in the presence of $NaBH_4$, whereas the tetraphenol strands with a *trans*-stilbene or *trans*-azobenzene unit did not form such a double-stranded helicate. The ^{1}H NMR and NOESY experiments revealed that *cis*-**3** adopted contracted (*cis*-$\mathbf{3_C}$) and extended (*cis*-$\mathbf{3_E}$) forms under equilibrium in CD_3CN at 25 °C. The contracted *cis*-$\mathbf{3_C}$ that accommodated a Na^+ ion in the center showed an almost reversible extension and contraction motion by removal and addition of a Na^+ ion. The *cis*-to-*trans* photoisomerisation of the extended *cis*-$\mathbf{3_E}$ with UV light (295 nm) further induced an extension of the helicate, producing a mixture of *cis*,*trans*-$\mathbf{3_E}$ and *trans*-$\mathbf{3_E}$ helicates at the photostationary state. However, *trans*-to-*cis* photoisomerisation of the *trans*-mixtures using UV light (360 nm) was irreversible in this system and produced the photooxidated aldehyde species (*trans*-**4**), resulting from the photo-cleavage of the *trans*-stilbene moieties of the *trans*-$\mathbf{3_E}$.

Introduction

The design and synthesis of functional molecules and polymers that exhibit a unidirectional molecular motion, such as rotary and elastic (extension and contraction) motions induced by external stimuli,[1] in particular by irradiation of light have attracted a great deal of attention in the past two or three decades,[2] because such photoresponsive molecular and polymeric systems can be applied for developing molecular motors,[2a-2d,2g,3] artificial muscles,[1i,1j,4] and molecular devices and materials.[2d-2f,5]

We previously reported a series of *ortho*-linked tetraphenol strands bearing a biphenol,[6] biphenylene (**1**),[7] bipyridine,[8] or bisporphyrin[9] unit in the middle that formed unique double-stranded helicates bridged by two spiroborates in which one[6,7] or two Na^+ cations[8] were accommodated in the center except for a large bisporphyrin-linked spiroborate helicate.[9] Conventional optical resolution of these helicates, such as diastereomeric salt formation or chiral high-performance liquid chromatography (HPLC) separation, provided pairs of optically pure enantiomers being stable toward racemisation. Among the helicates prepared so far, the optically active biphenylene-linked spiroborate helicate (**1**) showed an intriguing ion-triggered reversible extension and contraction motion coupled with a unidirectional twisting motion upon release and binding of Na^+ ions (Scheme 1A);[7a] the contracted helicate ($\mathbf{1_C}$) significantly extended through addition of [2.2.1]cryptand ([2.2.1]), resulting in the formation of extended helicate ($\mathbf{1_E}$) with a B–B distance of 13.0 Å that is more than two-fold when compared with that of the contracted $\mathbf{1_C}$ (6.0 Å). One might anticipate that if this unique spring-like motion could be controlled by irradiation of light, this would contribute to developing feasible nanoscale mechanical devices.[1g,2,5e]

To this end, we have designed and synthesized three novel *ortho*-linked tetraphenol strands linked by photoresponsive *cis*- and *trans*-stilbene[4b,10] and *trans*-azobenzene[10b,11] units in the middle (Scheme 2) and investigated their double-stranded helicate formations stabilised by spiroborates with $NaBH_4$. We found that only the *cis*-stilbene-containing tetraphenol strand yielded a desired double-stranded spiroborate helicate (*cis*-**3**), whereas the tetraphenol strands with a *trans*-stilbene or *trans*-azobenzene unit did not give such a helicate. We expected that the contracted helicate *cis*-$\mathbf{3_C}$ would undergo an extension (*cis*-$\mathbf{3_E}$) and contraction (*cis*-$\mathbf{3_C}$) motion by the Na^+ ion release and binding (chemical stimulus) as well as by light irradiation (physical stimulus) through *cis*-to-*trans* photoisomerisation of the stilbene units, thus producing *cis*-$\mathbf{3_E}$ and more extended *trans*-$\mathbf{3_E}$, respectively (Scheme 1B). Although this *cis*-*trans* photoisomerisation was irreversible because of the photo-cleavage of the *trans*-stilbene moieties under irradiation of light, to the best of our knowledge, wholly-artificial double helices showing a light-triggered spring-like motion are hitherto unknown.[4d,12,13]

[a] *Department of Molecular Design and Engineering, Graduate School of Engineering, Nagoya University, Chikusa-ku, Nagoya 464-8603, Japan. Fax: +81-52-789-3185; Tel: +81-52-789-4495; E-mail: yashima@apchem.nagoya-u.ac.jp*
[b] *Institut des Sciences Chimiques de Rennes, UMR 6226 CNRS-Université de Rennes 1, France.*

† Electronic Supplementary Information (ESI) available: Additional spectroscopic data. See DOI: 10.1039/b000000x/

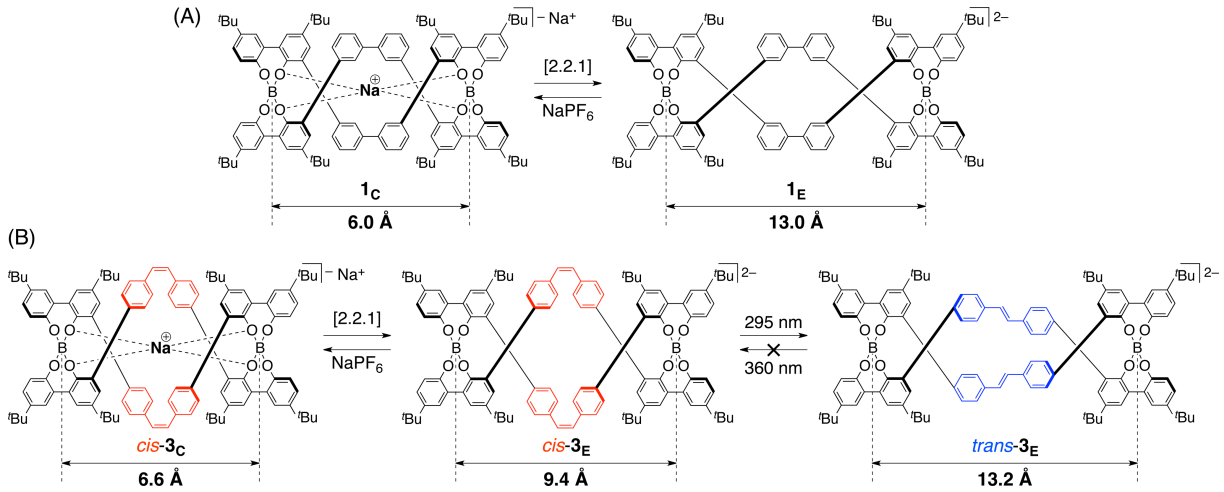

Scheme 1 Extension (**E**) and contraction (**C**) motions of spiroborate-based double-stranded helicates bearing biphenyl units (**1**) (A) and stilbene units (**3**) (B) in the middle. The contracted helicates ($\mathbf{1}_C$ and *cis*-$\mathbf{3}_C$) including a sodium ion in their helical cavities extend upon the addition of [2.2.1] ($\mathbf{1}_E$ and *cis*-$\mathbf{3}_E$). Further addition of $NaPF_6$ causes the formation of contracted forms. The *cis*-$\mathbf{3}_E$ is further extended upon *cis*-to-*trans* photoisomerisation.

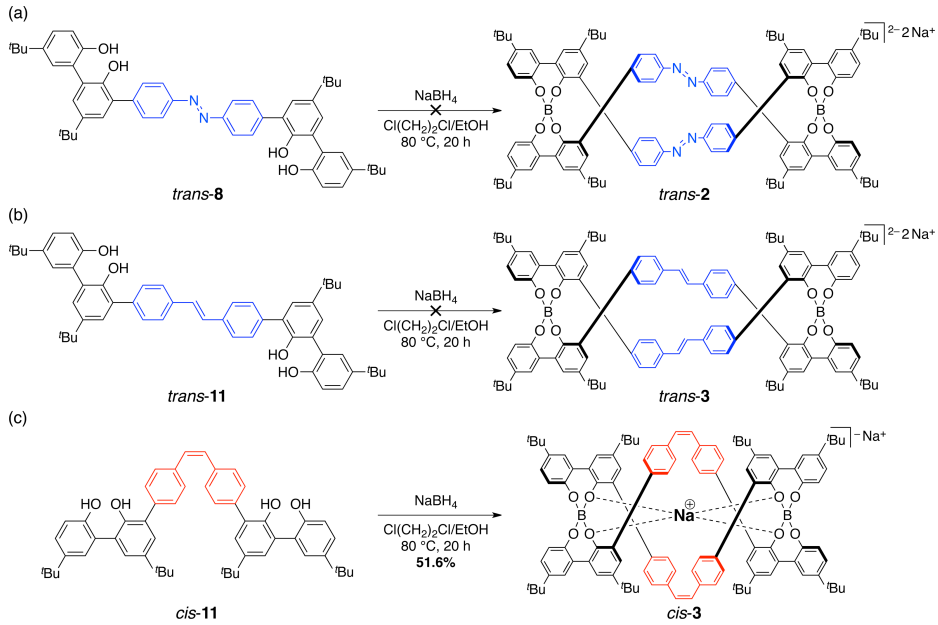

Scheme 2 Synthesis of spiroborate-based helicates bearing *trans*-azobenzene (*trans*-**2**) (a), *trans*-stilbene (*trans*-**3**) (b), and *cis*-stilbene (*cis*-**3**) (c) units in the middle.

Results and discussion

Synthesis of tetraphenol strands linked by photoresponsive units and the corresponding spiroborate helicates

The *trans*-azobenzene-containing tetraphenol (*trans*-**8**) was synthesised by Suzuki-Miyaura coupling of a boronic acid (**5**) with *trans*-4,4'-diiodoazobenzene (*trans*-**6**), subsequently followed by deprotection of the methoxy groups using BBr_3 according to a previously reported method[6-8] (Scheme S1 in ESI†). The *trans*- and *cis*-stilbene-containing tetraphenols (*trans*-**11** and *cis*-**11**, respectively) were also synthesised in a similar way by Suzuki-Miyaura coupling of a boronic acid ester (**9**)[9] with the corresponding *trans*- and *cis*-4,4'-diiodostilbenes (*trans*-**10** and *cis*-**10**, respectively) (Scheme S2 in ESI†).

The obtained tetraphenol strands were then allowed to react with an equimolar amount of $NaBH_4$ in 1,2-dichloroethane and ethanol (5/1, v/v) at 80 °C for 20 h under similar conditions used for the synthesis of the spiroborate helicates reported previously[6-8] (Scheme 2). However, the products from *trans*-**8** and *trans*-**11** were complicated based on their ^{1}H NMR spectra, and the electrospray ionisation (ESI) mass spectra in the negative mode indicated the formation of dimers and trimers bridged by one and two spiroborates, respectively, along with unreacted strands (Scheme 2a, b and Figs. S1 and S2 in ESI†), probably because the planar *trans*-azobenzene and *trans*-stilbene units hamper such a twisted spiroborate formation due to steric effects.

On the other hand, the *cis*-stilbene strand (*cis*-**11**) favourably reacted with $NaBH_4$, giving the corresponding helicate (*cis*-**3**) in 51.6% yield under the same condition (Scheme 2c) as supported by the ESI mass spectrum, which showed signals due to the

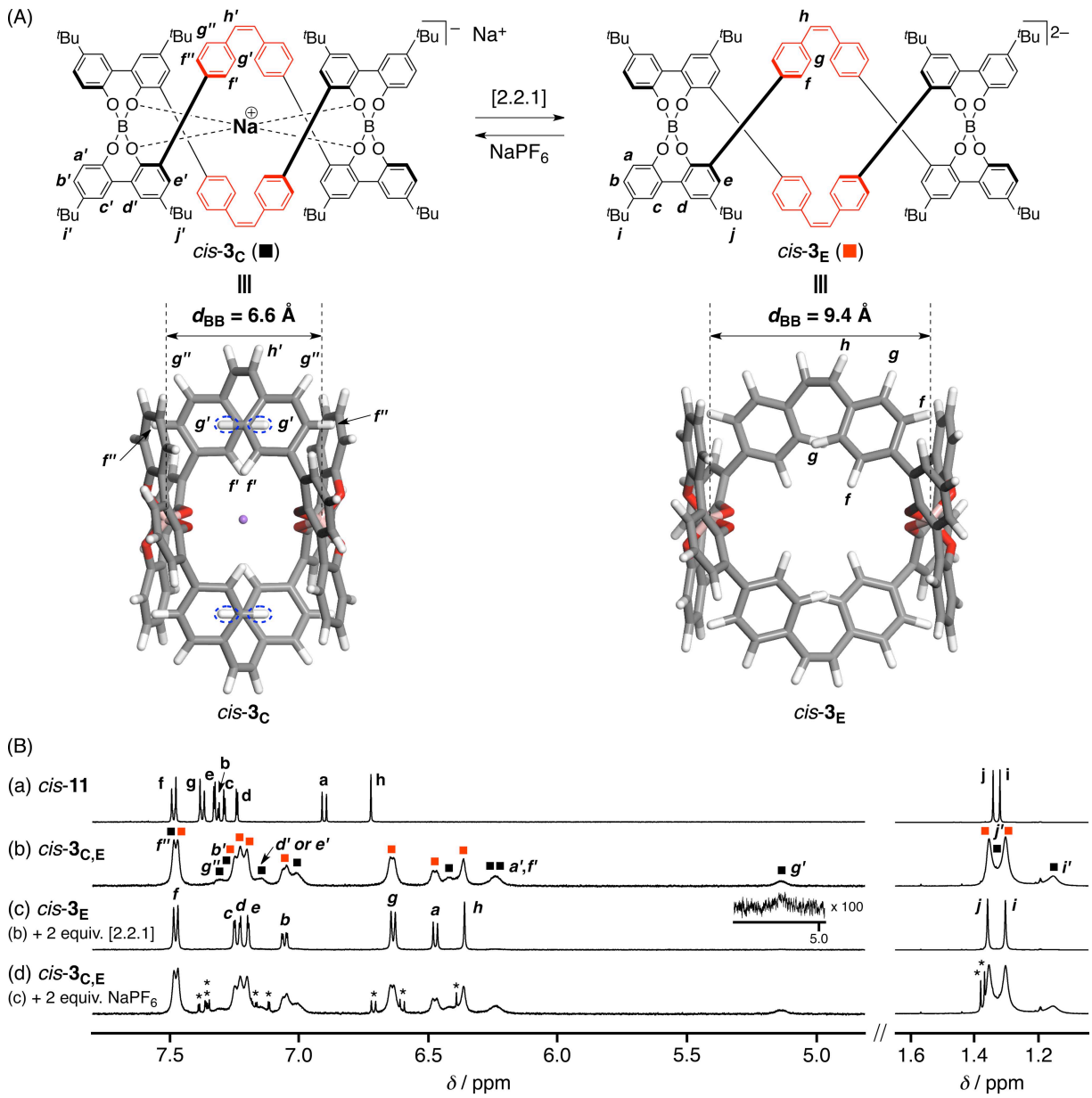

Fig. 1 (A) Optimised structures of left-handed helical *cis*-$\mathbf{3_C}$ (monoanion) and *cis*-$\mathbf{3_E}$ (dianion) calculated by Hartree-Fock method (6-31G*, CH_3CN), in which all the ^{t}Bu groups were substituted with hydrogen atoms for simplifying the calculations. (B) ^{1}H NMR spectra (500 MHz, CD_3CN, 25 °C) of *cis*-**11** (0.65 mM) (a), *cis*-**3** (0.31 mM) (b), (b) + 2 equiv. [2.2.1] (c), and (c) + 2 equiv. $NaPF_6$ (d). B and B denote the signals for the contracted (*cis*-$\mathbf{3_C}$) and extended (*cis*-$\mathbf{3_E}$) helicates, respectively. The peak assignments were done on the basis of gCOSY and NOESY spectra (Figs. S5–S8 in ESI†). * denotes the signals tentatively assigned to the *meso*-*cis*-$\mathbf{3_E}$ (see the text and Figs. S9 and S10 in ESI†).

monovalent (*cis*-$\mathbf{3}^-$) and divalent (*cis*-$\mathbf{3}^{2-}$) anions at m/z = 1581.75 and 779.36, respectively (Fig. S3 in ESI†).

Extension and contraction motion of *cis*-3

Figs. 1B (a and b) show the ^{1}H NMR spectra of *cis*-**11** and *cis*-**3**, respectively, measured in CD_3CN at 25 °C. Interestingly, most of the proton resonances for *cis*-**3** appeared as two sets of nonequivalent broadened signals after spiroborate helicate formation (B and B, b in Fig. 1B); such nonequivalent proton resonances have not been observed for the other spiroborate helicates prepared so far.[6-9] In order to assign these signals, 2 equiv. of [2.2.1] were added to a solution of *cis*-**3**. As shown in c in Fig. 1B, the broad signals became sharper ones, while maintaining their chemical shifts (B) along with significant decrease in the signals marked by B in c in Fig. 1B. As reported previously, the Na^+ ion weakly bound in the contracted helicate ($\mathbf{1_C}$) could be released quantitatively in the presence of [2.2.1], resulting in the formation of the extended helicate ($\mathbf{1_E}$) (Scheme 1A).[7a] Based on these observations, the two sets of nonequivalent signals (B and B, b in Fig. 1B) could be reasonably assigned to those of the contracted (*cis*-$\mathbf{3_C}$) and extended (*cis*-$\mathbf{3_E}$) forms, respectively, which indicates that the Na^+ ion binding and release rates, in other words, the corresponding contracted and extended motions of *cis*-**3** are slow in CD_3CN on the ^{1}H NMR time scale, giving separated signals under equilibrium (b in Fig. 1B), from which the ratio of *cis*-$\mathbf{3_C}$ to *cis*-$\mathbf{3_E}$ and its equilibrium constant (K) were estimated to be 30 : 70 and 2 x 10^3 M^{-1}, respectively. In the presence of [2.2.1] (2 equiv.), the ratio of *cis*-$\mathbf{3_C}$ to *cis*-$\mathbf{3_E}$ changed

Table 1 Results of the photoisomerisation of *cis*-**11** and *cis*-**3** in CD_3CN upon irradiation of UV light at 295 and subsequently at 360 nm

	11[a,b]	**3**[a,c]				
	cis-**11** : *trans*-**11**	*cis*-**3** / %	*cis,trans*-$\mathbf{3_E}$ / %	*trans*-$\mathbf{3_E}$ / %	*trans*-**4** / %	*cis* : *trans*[d]
Before irradiation	99 : 1	97	3	0	0	98.5 : 1.5
After irradiation with 295 nm light (*cis*-to-*trans*)	8 : 92	21	39	38	2	40.5 : 58.5
After irradiation with 360 nm light (*trans*-to-*cis*)	42 : 56[e]	24	43	20	13	45.5 : 48.0

[a] Product ratios were estimated by ^{1}H NMR analyses. [b] 0.65 mM at 25 °C under air (see Figs. S11 and S12 in ESI†). [c] 0.25 mM *cis*-**3** in the presence of 2 equiv. [2.2.1] at 25 °C under argon (see Fig. 3 and Fig. S15 in ESI†). [d] Overall *cis* and *trans* ratio of the stilbene units of **3** and **4**. [e] A trace amount of oxidised aldehydes (ca. 2%) was produced during the photoisomerisation (see Fig. S11b in ESI†).

to be approximately 10 : 90 (c in Fig. 1B). The further addition of [2.2.1] (3 equiv.) brought about the complete shift of the equilibrium to the extended helicate formation (*cis*-$\mathbf{3_E}$).

According to this assignment, the upfield shifts of some aromatic protons for *cis*-**3**, in particular those for *cis*-$\mathbf{3_C}$ (b in Fig. 1B), were explained by the shielding effect of the benzene rings of the other strand as observed in the other spiroborate helicates.[6-9] The upfield shift of the stilbene protons (g') was more significant. The calculated structures of *cis*-$\mathbf{3_C}$ and *cis*-$\mathbf{3_E}$ in CH_3CN by using the Hartree-Fock method (HF, 6-31G*) support the upfield shifts of the stilbene protons (g') of *cis*-$\mathbf{3_C}$, which are favourably positioned above the benzene rings of the twisted stilbene residues into one direction (Fig. 1A). The energy difference (ΔG_{Cal}) between the calculated structures in CH_3CN revealed that the *cis*-$\mathbf{3_E}$ is 2 kcal mol^{-1} more stable than the *cis*-$\mathbf{3_C}$ (Fig. 1A), which is consistent with the major species (*cis*-$\mathbf{3_E}$) observed by the ^{1}H NMR spectrum of *cis*-**3** in CD_3CN at 298 K at equilibrium (b in Fig. 1B).

The equilibrium between *cis*-$\mathbf{3_C}$ and *cis*-$\mathbf{3_E}$ was also unambiguously confirmed by the concentration-dependent ^{1}H NMR and 2D NOESY (2D exchange spectroscopy (EXSY)) spectra of *cis*-**3** in the absence and presence of [2.2.1] (2 equiv.), respectively.[14] The intensities of the signals (B) derived from *cis*-$\mathbf{3_C}$ gradually decreased with the decrease in the concentration of *cis*-**3** (0.31−0.080 mM), whereas those of the signals (B) due to *cis*-$\mathbf{3_E}$ relatively increased and the signals became sharper without any changes in their chemical shifts (Fig. S4 in ESI†), from which the *K* value was also estimated to be 2 x 10^3 M^{-1}, indicating that the equilibrium involves the sodium ion release and binding. In addition, the 2D NOESY (EXSY) spectrum of *cis*-**3** with 2 equiv. of [2.2.1] showed clear positive exchange cross-peaks between the two species, contracted *cis*-$\mathbf{3_C}$ (B) and extended *cis*-$\mathbf{3_E}$ (B) forms as well as negative intrastrand NOE cross-peaks for *cis*-$\mathbf{3_E}$ (Figs. S6-S8 in ESI†). Although interstrand NOE cross-peaks were not observed for *cis*-$\mathbf{3_E}$, a similar tendency was reported for the other extended spiroborate helicates.[7a]

The subsequent addition of $NaPF_6$ to the solution of *cis*-$\mathbf{3_E}$ in the presence of 2 equiv. of [2.2.1] (d in Fig. 1B) regenerated the original helicates as a mixture of *cis*-$\mathbf{3_C}$ and *cis*-$\mathbf{3_E}$, while new sharp signals different from those of the ligand *cis*-**11** and the helicates (*cis*-$\mathbf{3_C}$ and *cis*-$\mathbf{3_E}$) appeared in the aromatic and *t*-Bu proton resonance regions; the content of the new species was ca. 6% (d in Fig. 1B). We found that the identical new species also formed when a CD_3CN solution of *cis*-**3** was allowed to stand for a long time (Fig. S9A in ESI†); its ESI mass spectrum (Fig. S10 in ESI†) was identical to that measured just after dissolving *cis*-**3** in CH_3CN (Fig. S3 in ESI†). These results together with the COSY spectrum of a CD_3CN solution of *cis*-**3** after standing for ca. 36 h (Fig. S9B in ESI†) suggest that the new species is a structural isomer of the *racemo*-helicates (*cis*-$\mathbf{3_C}$ and *cis*-$\mathbf{3_E}$) and is most likely a double-stranded *meso*-helicate with an extended structure (*meso*-*cis*-$\mathbf{3_E}$) that will be generated from the *racemo*-helicates in solution and reached an equilibrium within a few days. Indeed, calculations predict that *meso*-*cis*-$\mathbf{3_E}$ is 2.7 kcal mol^{-1} more stable than *cis*-$\mathbf{3_E}$ (Table S1 in ESI†). Although the mechanism for the present *racemo*-to-*meso*-*cis*-**3** isomerisation, which requires the breaking and reformation process of the spiroborate groups, remains unknown, these results revealed that the *racemo*-*cis*-**3** exists as a mixture of the interconvertible contracted (*cis*-$\mathbf{3_C}$) and extended (*cis*-$\mathbf{3_E}$) forms in solution and that the ion-triggered extension and contraction motion mostly proceeds reversibly; however, the present system seems to be more complicated than before, and involves the other chemical equilibrium, *i.e.,* *racemo*-to-*meso*-*cis*-**3** isomerisation. Apparently, a further study is necessary to unambiguously elucidate the structure of the *meso*-*cis*-$\mathbf{3_E}$ by single-crystal X-ray analysis and the mechanism of this unexpected isomerisation.

Photoisomerisation of *cis*-11

Cis/*trans* photoisomerisation of the single strand *cis*-**11** was first investigated by ^{1}H NMR and absorption spectroscopies in CD_3CN (Figs. S11-S12 and S13-S14, respectively in ESI†). Upon irradiation of UV light at 295 nm, the intensities of the *cis*-**11** protons decreased with time, while the new peaks due to *trans*-**11** appeared with a gradual increase in their intensities and the *cis*/*trans* ratio reached a constant value (8 : 92) after irradiation for 120 min as estimated from the integral ratio of the *cis*- and *trans*-stilbene protons (f_c and g_t) (Table 1 and Fig. S11a in ESI†). Subsequent irradiation with UV light at 360 nm, which induces the *trans*-to-*cis* isomerisation, produced a mixture of *cis*- and *trans*-**11** (Fig. S11b in ESI†); its ratio changed with time and reached an almost constant value (42 : 56) at the photostationary state after 120 min irradiation (Table 1 and Fig. S12 in ESI†), indicating that the *trans*-to-*cis* photoisomerisation did not take place efficiently as reported for typical stilbene derivatives.[15]

The changes in the absorption spectra of *cis*-**11** in a dilute CD_3CN solution during the course of the *cis*-to-*trans* followed by the *trans*-to-*cis* photoisomerisations were also measured (Fig. S13 in ESI†). An absorption peak at 335 nm due to the formation of *trans*-**11** gradually increased with time accompanied with a

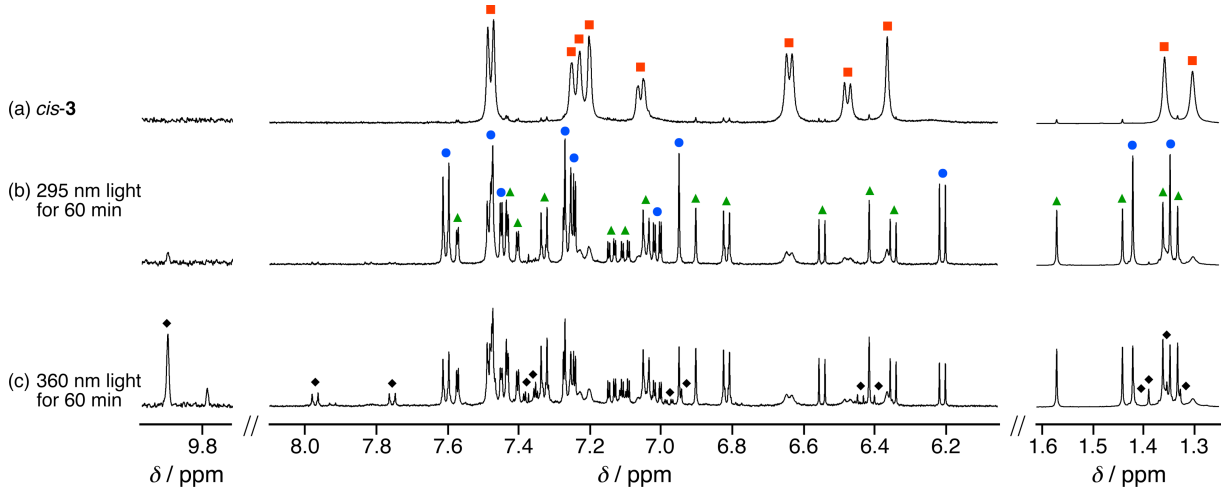

Fig. 2 ^{1}H NMR spectral changes of *cis*-**3** (500 MHz, CD_3CN, 25 °C, 0.25 mM) in the presence of 2 equiv. [2.2.1] before (a) and after irradiation of UV light at 295 nm for 60 min (b), followed by irradiation of UV light at 360 nm for 60 min under argon (c) (see Fig. S15 in ESI†). B, H, J, and F denote the signals for *cis*-$\mathbf{3_E}$, *cis*,*trans*-$\mathbf{3_E}$, *trans*-$\mathbf{3_E}$, and *trans*-**4**, respectively. The peak assignments were done on the basis of the ESI-MS spectrum of the mixture (Fig. S16 in ESI†) and gCOSY and NOESY spectra (Figs. S17–S19 in ESI†).

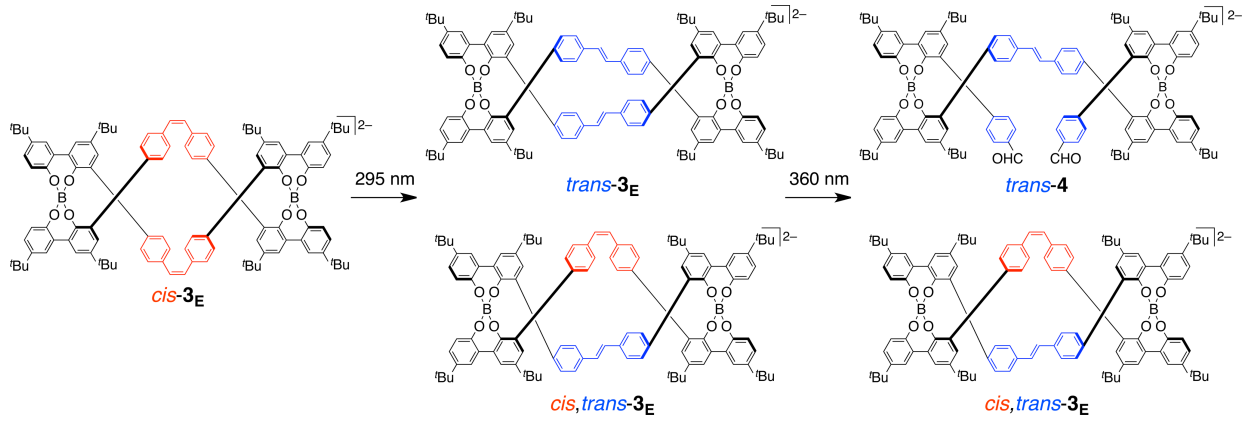

Scheme 3 Photoisomerisation of *cis*- and *trans*-stilbene helicates.

clear isosbestic point at 298 nm upon irradiation of UV light at 295 nm, affording the *trans*-**11** in 94% yield. Further irradiation with UV light at 360 nm gave a mixture of *cis*- and *trans*-**11** (43 : 57) at the photostationary state (Fig. S13b and c in ESI†); the *cis*/*trans* ratio was estimated by using a calibration curve obtained from the plots for the absorption intensity ratio at 335 and 298 nm as a function of the *trans*-**11** content estimated from the ^{1}H NMR analyses. The results were fully consistent with those obtained from the ^{1}H NMR analyses, although a trace amount of a photooxidised product (aldehydes) (ca. 2%) was produced upon irradiation of UV light at 360 nm under air as shown in Fig. S11 (ESI†). As anticipated, the fluorescence intensity of **11** significantly increased during the *cis*-to-*trans* photoisomerisation (Fig. S14b in ESI†).

Photoisomerisation of *cis*-3

With all the above photoisomerisation results of *cis*-**11** in mind, we then investigated the photoisomerisation behaviour of the double-stranded helicate *cis*-**3** composed of two *cis*-**11** strands with ^{1}H NMR and absorption spectroscopies in a manner similar to that for *cis*-**11**. Fig. 2 shows the ^{1}H NMR spectral changes of *cis*-**3** in CD_3CN in the presence of 2 equiv. of [2.2.1] before and

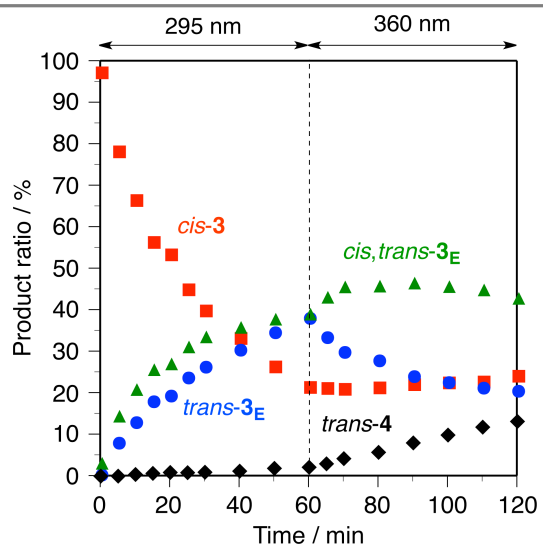

Fig. 3 Time-dependent changes in the product ratio during the photoisomerisation of *cis*-**3** (0.25 mM) in the presence of 2 equiv. [2.2.1] upon irradiation of UV light at 295 nm, followed by irradiation of UV light at 360 nm under argon (see Fig. S15 in ESI†).

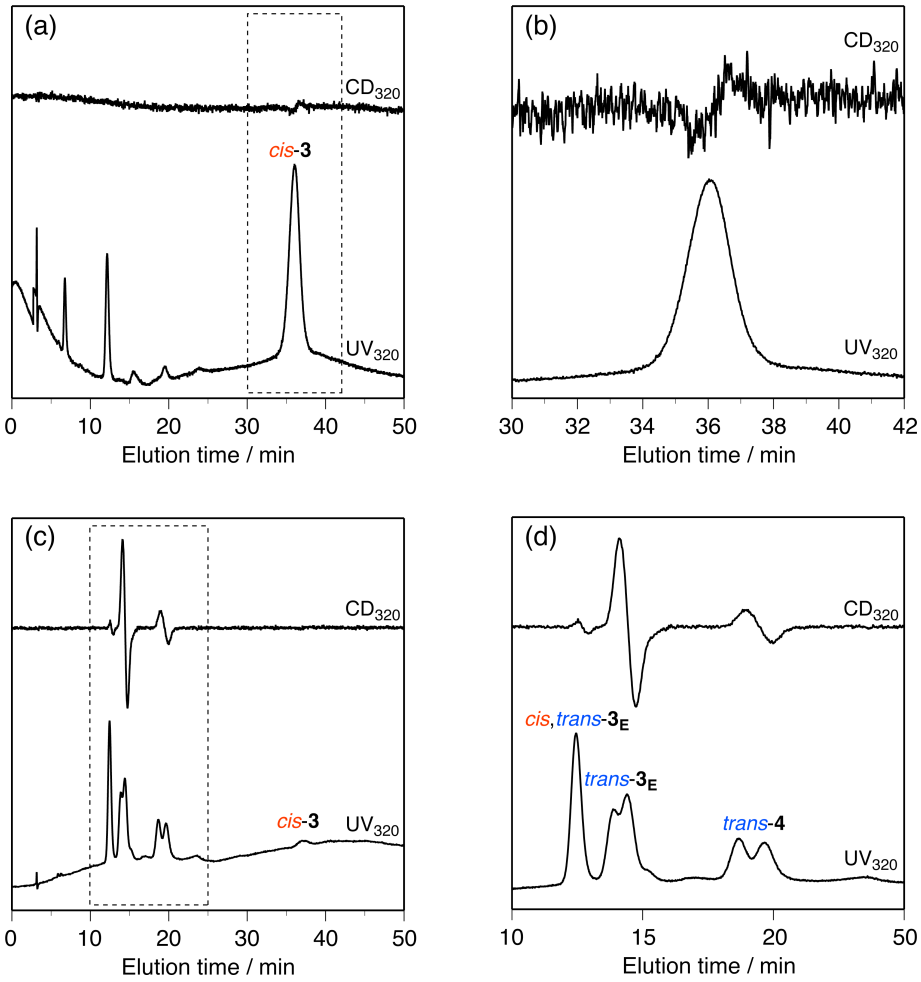

Fig. 4 HPLC chromatograms for the resolution of *cis*-**3** in CH_3CN (a) and *cis*-$\mathbf{3_E}$ in the presence of 7 equiv. [2.2.1] in CD_3CN after irradiation of UV light at 295 nm for 90 min under air (c) (see Fig. S21b in ESI†). Magnified chromatograms corresponding to the areas indicated by the squares in (a) and (c) are shown in (b) and (d), respectively. HPLC conditions: column, Chiralpak IB (Daicel, 0.46 (i.d.)×25 cm); eluent: hexane/$CHCl_3$ (6:4, v/v) containing 0.5 mg/mL tetrabutylammonium bromide (TBAB); flow rate, 1.0 mL min^{-1}; column temperature, 25 °C. The peak assignments were performed by fractionation of each peak, followed by measurements of the ^{1}H NMR spectra. We note that photoirradiation of *cis*-$\mathbf{3_E}$ in air produced a larger amount of the photooxidised *trans*-**4**.

after irradiation of UV light at 295 nm followed by 360 nm for 60 min each (for more detailed time-dependent ^{1}H NMR spectral changes and the product ratio changes, see Fig. S15 in ESI† and Fig. 3, respectively).

In sharp contrast to *cis*-**11**, the ^{1}H NMR spectrum of *cis*-**3** became quite complicated after irradiation of UV light at 295 nm for 60 min (Fig. 2b) because of newly generated *cis*,*trans*-$\mathbf{3_E}$ and *trans*-$\mathbf{3_E}$ as well as the unreacted *cis*-$\mathbf{3_E}$ (Scheme 3), suggesting that the *cis*-to-*trans* isomerisation in this system was less efficient presumably because of the highly strained, covalently-bonded spiroborated duplex structure (Fig. 1A); the product ratio estimated by its ^{1}H NMR spectrum (Fig. 2b) was *cis*,*trans*-$\mathbf{3_E}$ (39%) and *trans*-$\mathbf{3_E}$ (38 %) along with a small amount of *trans*-**4** (2%) (Table 1, see below). However, it should be emphasised that the *trans*-$\mathbf{3_E}$, which was not directly synthesised by the reaction of *trans*-**11** with $NaBH_4$ under the conditions used for the synthesis of spiroborate helicates[6-8,16] (Scheme 2), was successfully produced via *cis*-to-*trans* photoisomerisation of the corresponding *cis*-**3**. Subsequent irradiation of UV light at 360 nm further produced a new set of proton resonances with a characteristic singlet at 9.84 ppm (Fig. 2c), which could be derived from an aldehyde species (*trans*-**4**) most likely generated by photooxidation of *trans*-$\mathbf{3_E}$ in the presence of trace amounts of oxygen.[17] The dialdehyde (*trans*-**4**) formation that was evidenced by the negative ESI-mass spectrum (Fig. S16B in ESI†) unfortunately caused the irreversible *trans*-*cis* photoisomerisation of this system, and its content increased with time (Fig. S15 in ESI† and Table 1).

The photo-induced *cis*/*trans* isomerisation of *cis*-$\mathbf{3_E}$ was also investigated by absorption spectroscopy. Similar time-dependent absorption spectral changes of *cis*-$\mathbf{3_E}$ in a dilute CD_3CN solution containing 3 equiv. of [2.2.1] were observed during the course of the *cis*-to-*trans* and *trans*-to-*cis* photoisomerisations, but the changes were not significant as compared to those of *cis*-**11** because of inefficient *cis*-to-*trans* isomerisation and oxidation that took place during the *trans*-to-*cis* photoisomerisation, giving the oxidized *trans*-**4** (Fig. S20a, b in ESI†). The fluorescence intensity of *cis*-$\mathbf{3_E}$ was also enhanced upon irradiation of UV light (295 nm), resulting in the formation of a mixture of *cis*,*trans*-$\mathbf{3_E}$, *trans*-$\mathbf{3_E}$, and *trans*-**4** (Fig. S20c, d in ESI†).

Optical resolution of helicates

As mentioned above, the *cis*-**3** just after preparation undergoes the ion-triggered extension and contraction motion in acetonitrile, which further changes its structure to a new species in acetonitrile under equilibrium. We tentatively assigned the *cis*-**3** and the new species as *racemo*- and *meso*-*cis*-$\mathbf{3_E}$ helicates, respectively, on the basis of their NMR spectra. Obviously, the *racemo*-*cis*-**3** helicate is chiral, whereas the *meso*-*cis*-$\mathbf{3_E}$ helicate is achiral, and in order to confirm these structural assignments, we investigated if the chiral *cis*-**3** could be resolved into enantiomers by HPLC using a chiral column (Chiralpak IB, Daicel).

Fig. 4a shows the chromatogram of the resolution of *cis*-**3**, showing a single peak detected by UV, although the circular dichroism (CD)-detected chromatogram indicated a partial separation with negative and positive CDs; their CD intensities were too weak to evidence the enantioseparation (Fig. 4b). Next, a CH_3CN solution of a mixture of *cis*,*trans*-$\mathbf{3_E}$, *trans*-$\mathbf{3_E}$, and *trans*-**4** prepared from *cis*-$\mathbf{3_E}$ through the photoisomerisation under air was injected into the chiral HPLC system (Fig. S21 in ESI†). As shown in Fig. 4d, the *trans*-$\mathbf{3_E}$ and *trans*-**4** were not completely but rather were partially separated into a pair of enantiomers with the first positive and second negative CD signs. Importantly, the *trans*-$\mathbf{3_E}$ and *trans*-**4** were converted from *cis*-$\mathbf{3_E}$ via photoisomerisation without any breaking and reformation process of the spiroborate groups, leading to the conclusion that the *cis*-**3** is a *racemo*-helicate with a double-stranded spiroborate structure and the new species formed from the *cis*-**3** in CD_3CN may possess a *meso* structure.

Conclusions

In summary, we have successfully synthesised the photoresponsive spiroborate-based double-stranded helicate (*cis*-**3**) bearing *cis*-stilbene units in the middle, which underwent an extension (*cis*-$\mathbf{3_E}$) and contraction (*cis*-$\mathbf{3_C}$) motion by the Na^+ ion release and binding. Although photo-induced *cis*/*trans* isomerisation of *cis*-**3** did not efficiently nor reversibly take place because of its highly strained spiroborated duplex structure in addition to the oxidative photo-cleavage of the *trans*-stilbene moieties under irradiation of UV light, the present results provide further design strategy for developing novel photoresponsive spiroborate-based helicates that exhibit light-triggered spring-like motions by introducing an overcrowded double bond into the helicates as a photo- and thermo-responsive linker.[2a,2c,2g,3]

Experimental section

1. Materials and instruments

Materials. All starting materials and dehydrated solvents were purchased from commercial suppliers and were used without further purification unless otherwise noted. Silica gel (SiO_2) for the flash chromatography was purchased from Merck. The boronic acid (**5**),[18] (*E*)-4,4'-diiodoazobenzene (**6**),[19] the boronic acid pinacol ester (**9**),[9] and (*Z*)-4,4'-diiodostilbene (**10**)[20] were prepared according to the literature.

Instruments. The melting points were measured on an MPA100 OptiMelt automated melting point apparatus or a Yanaco MP-500D melting point apparatus (Kyoto, Japan), and were uncorrected. The NMR spectra were obtained using a Varian UNITY INOVA 500AS spectrometer operating at 500 MHz for ^1H and 125 MHz for ^{13}C or a Varian INOVA 700 spectrometer operating at 700 MHz for ^1H and 175 MHz for ^{13}C using tetramethysilane (TMS) or a solvent residual peak as the internal standard. The electron spray ionization (ESI) mass spectra were recorded using a JEOL JMS-T100CS spectrometer (Akishima, Japan). The absorption spectra were measured in a 1- or 10-mm quartz cell on a JASCO V-570 spectrophotometer. The photoirradiation for *cis*/*trans* isomerisation was performed on a JASCO FP-6500 spectrofluorometer with a 150 W xenon lamp under argon unless otherwise noted. The slit width used in the experiments was 20 nm. The chiral HPLC analyses were performed on a JASCO PU-2080 liquid chromatograph equipped with UV-visible (JASCO MD-2010) and CD detectors (JASCO CD-2095) using a Chiralpak IB column (0.46 (i.d.) x 25 cm, Daicel, Osaka, Japan).

2. Synthetic procedures

***trans*-7.** To a mixture of **5** (427 mg, 1.15 mmol), *trans*-**6** (200 mg, 0.461 mmol), and $Pd(PPh_3)_4$ (133 mg, 0.115 mmol) in toluene (7.2 mL) was added 2 M aqueous K_2CO_3 (7.2 mL). The reaction mixture was stirred at 110 °C for 36 h under nitrogen. After being cooled to room temperature, the mixture was extracted with EtOAc. The organic layer was washed with H_2O and dried over anhydrous $MgSO_4$. After filtration, the solvent was evaporated under reduced pressure. The crude product was purified by flash chromatography (SiO_2, 12 g) with *n*-hexane/EtOAc (10/0 to 10/1 (v/v)) to afford *trans*-**7** (289 mg, 75.5% yield) as an orange solid. Mp: 275.1–276.0 ºC. ^1H NMR (500 MHz, $CDCl_3$, r.t.): δ 8.00 (d, J = 8.5 Hz, 4H, ArH), 7.80 (d,

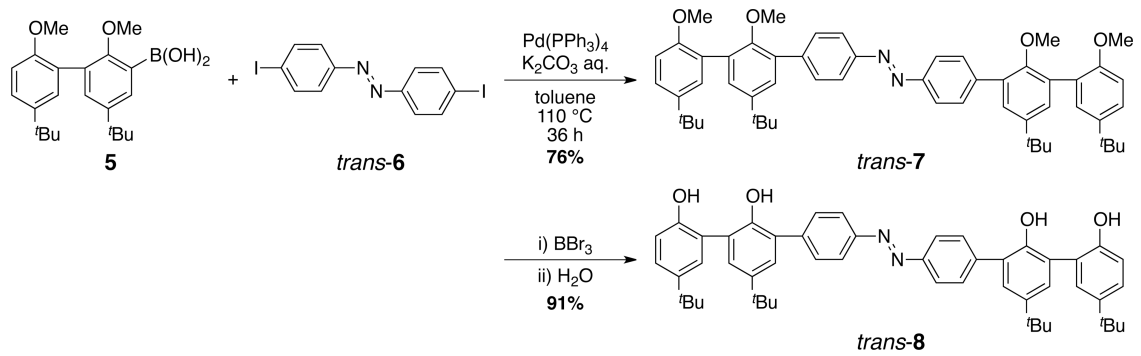

Scheme 4 Synthesis of *trans*-azobenzene ligand (*trans*-**8**).

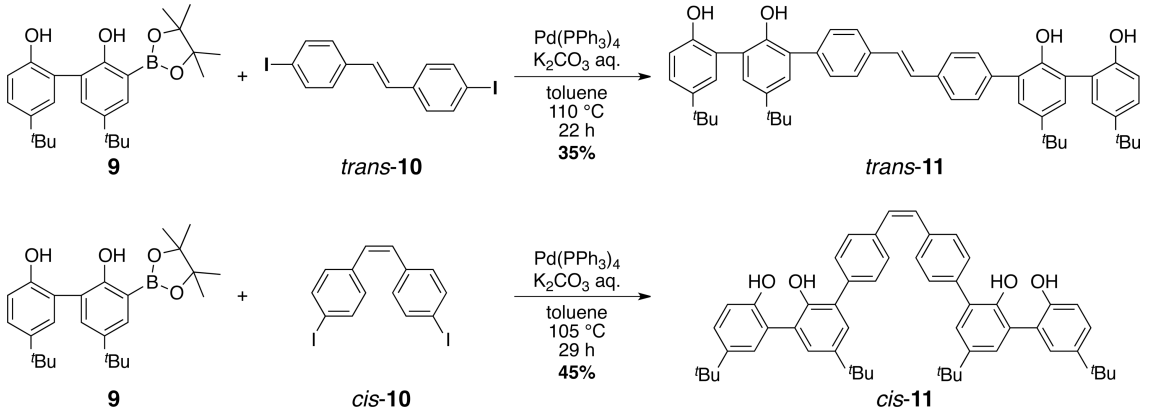

Scheme 5 Synthesis of stilbene ligands (*trans*-**11** and *cis*-**11**).

J = 8.5 Hz, 4H, ArH), 7.40–7.36 (m, 8H, ArH), 6.95 (d, J = 8.5 Hz, 2H, ArH), 3.81 (s, 6H, OCH_3), 3.24 (s, 6H, OCH_3), 1.38 (s, 18H, $C(CH_3)_3$), 1.34 (s, 18H, $C(CH_3)_3$). ^{13}C NMR (125 MHz, $CDCl_3$, r.t.): δ 154.79, 153.46, 151,78, 146.06, 143.12, 142.62, 133.36, 132.33, 130.25, 129.30, 129.05, 127.61, 127.34, 125.32, 122.86, 110.69, 60.73, 55.90, 34.64, 34.30, 31.74, 31.68. HRMS (positive mode ESI): m/z calcd for $[M(C_{56}H_{66}N_2O_4)+Na^+]^+$, 853.4920; found 853.4922.

***trans*-8.** To a solution of *trans*-**7** (200 mg, 0.241 mmol) in CH_2Cl_2 (5.0 mL) was added a CH_2Cl_2 solution of BBr_3 (1.0 M, 2.41 mL, 2.41 mmol) at -78 °C under nitrogen. After being warmed to room temperature, the reaction mixture was stirred for 19 h. The mixture was then quenched with H_2O (10 mL) at 0 °C and stirred at room temperature for 1 h. After the solvent was evaporated, the residue was extracted with EtOAc. The organic layer was washed with H_2O and dried over anhydrous $MgSO_4$. After filtration, the solvent was evaporated under reduced chromatography with *n*-hexane/EtOAc (10/0 to 10/1 (v/v)) to afford *trans*-**8** (170 mg, 90.9% yield) as a dark orange solid. Mp: 156.5–158.1 ºC (dec). ^{1}H NMR (500 MHz, $CDCl_3$, r.t.): δ 8.06 (d, J = 8.5 Hz, 4H, ArH), 7.77 (d, J = 8.5 Hz, 4H, ArH), 7.44 (d, J = 2.5 Hz, 2H, ArH), 7.38 (dd, J = 2.5, 8.5 Hz, 2H, ArH), 7.33 (m, 4H, ArH), 7.01 (d, J = 8.5 Hz, 2H, ArH), 5.55 (s, 2H, ArOH), 5.47 (s, 2H, ArOH), 1.39 (s, 18H, $C(CH_3)_3$), 1.35 (s, 18H, $C(CH_3)_3$). ^{13}C NMR (125 MHz, $CDCl_3$, r.t.): δ 152.03, 151.13, 147.67, 144.58, 144.49, 141.02, 130.35, 128.38, 128.15, 128.08, 128.00, 127.23, 124.26, 123.42, 123.41, 116.56, 34.55, 34.43, 31.71 (19 signals out of 20 expected ones). HRMS (negative mode ESI): m/z calcd for $[M(C_{52}H_{58}N_2O_4)–H^+]^-$, 773.4318; found 773.4311.

***trans*-11.** To a solution of **9** (93 mg, 0.22 mmol), *trans*-**10** (43 mg, 0.10 mmol), and $Pd(PPh_3)_4$ (23 mg, 0.020 mmol) in toluene (5.0 mL) was added 2 M aqueous K_2CO_3 (5.0 mL). The reaction mixture was stirred at 110 °C for 22 h under nitrogen. After being cooled to room temperature, the mixture was extracted with EtOAc. The organic layer was washed with H_2O and aqueous HCl, and dried over anhydrous $MgSO_4$. After filtration, the solvent was evaporated under reduced pressure. The crude product was purified by flash chromatography (SiO_2, 12 g) with *n*-hexane/EtOAc (10/0 to 6/4 (v/v)) to afford *trans*-**11** (27 mg, 35% yield) as a white solid. ε_{298}: 2.73 x 10^5 M^{-1} cm^{-1}. Mp: 152.8–155.6 ºC. ^{1}H NMR (500 MHz, $CDCl_3$, r.t.) δ 7.67 (d, J = 8.5 Hz, 4H, ArH), 7.59 (d, J = 8.5 Hz, 4H, ArH), 7.39 (d, J = 2.5 Hz, 2H, ArH), 7.37 (dd, J = 2.5, 8.5 Hz, 2H, ArH), 7.33 (d, J = 2.5 Hz, 2H, ArH), 7.31 (d, J = 2.5 Hz, 2H, ArH), 7.23 (s, 2H, HC=CH), 7.01 (d, J = 8.5 Hz, 4H, ArH), 5.56 (s, 2H, OH), 5.52 (s, 2H, OH), 1.37 (s, 18H, $C(CH_3)_3$), 1.34 (s, 18H, $C(CH_3)_3$). ^{13}C NMR (125 MHz, $CDCl_3$, r.t.): δ 151.23, 147.34, 144.54, 144.32, 137.24, 136.89, 129.86, 128.72, 128.36, 128.15, 127.81, 127.20, 127.05, 124.20, 123.91, 116.67, 34.53, 34.41, 31.72, 31.71 (20 signals out of 21 expected ones). HRMS(ESI): m/z calcd for $[M(C_{54}H_{60}O_4)–H^+]^-$, 771.4413; found 771.4379.

***cis*-11.** To a solution of **9** (216 mg, 0.509 mmol), *cis*-**10** (100 mg, 0.231 mmol), and $Pd(PPh_3)_4$ (58.8 mg, 0.0509 mmol) in toluene (5.0 mL) was added 2 M aqueous K_2CO_3 (5.0 mL). The reaction mixture was stirred at 105 °C for 29 h under nitrogen. After being cooled to room temperature, the mixture was extracted with EtOAc. The organic layer was washed with H_2O and dried over anhydride $MgSO_4$. After filtration, the solvent was evaporated under reduced pressure. The crude product was purified by flash chromatography (SiO_2, 12 g) with *n*-hexane/EtOAc (10/0 to 8/2 (v/v)) to afford *cis*-**11** (80.0 mg, 44.7% yield) as a white solid. ε_{298}: 2.73 x 10^5 M^{-1} cm^{-1}. Mp: 136.5–138.9 ºC. ^{1}H NMR (500 MHz, $CDCl_3$, r.t.) δ 7.48–7.45 (m, 8H, ArH), 7.36 (d, J = 2.5 Hz, 2H, ArH), 7.35 (dd, J = 2.5, 8.5 Hz, 2H, ArH), 7.31 (d, J = 2.4 Hz, 2H, ArH), 7.29 (d, J = 2.5 Hz, 2H, ArH), 6.99 (d, J = 8.5 Hz, 2H, ArH), 6.68 (s, 2H, HC=CH), 5.57 (s, 2H, OH), 5.54 (s, 2H, OH), 1.35 (s, 18H, $C(CH_3)_3$), 1.33 (s, 18H, $C(CH_3)_3$). ^{13}C NMR (125 MHz, $CDCl_3$, r.t.): δ 151.22, 147.28, 144.49, 144.26, 136.74, 136.73, 130.27, 129.59, 129.38, 128.30, 128.13, 128.11, 127.80, 127.00, 124.14, 123.93, 116.62, 34.51, 34.39, 31.71, 31.70. HRMS(ESI): m/z calcd for $[M(C_{54}H_{60}O_4)–H^+]^-$, 771.4413; found 771.4380.

***trans*-2.** To a solution of *trans*-**8** (3.0 mg, 3.9 μmol) in 1,2-dichloroethane (625 μL) was added a solution of $NaBH_4$ in ethanol (31.2 mM, 125 μL, 3.90 μmol). The reaction mixture was stirred at 80 °C for 20 h under argon. After being cooled to room temperature, the solvents were evaporated under reduced pressure and the residue was dried in vacco. The negative ESI mass spectrum of the residue dissolved in CD_3CN was then measured using CH_3CN as the eluent (Fig. S1 in ESI†).

***trans*-3.** To a solution of *trans*-**11** (3.3 mg, 4.3 μmol) in 1,2-dichloroethane (486 μL) was added a solution of $NaBH_4$ in ethanol (44.0 mM, 98 μL, 4.3 μmol). The reaction mixture was

stirred at 80 °C for 20 h under argon, resulting in a precipitate. After being cooled to room temperature, the solvents were evaporated under reduced pressure and the residue was dried in vacco. The negative ESI mass spectrum was measured after the residue was dissolved in DMSO-d_6 and then diluted with CH_3CN (Fig. S2 in ESI†).

***cis*-3.** To a solution of *cis*-**11** (20.5 mg, 26.5 μmol) in 1,2-dichloroethane (3.0 mL) was added a solution of $NaBH_4$ in ethanol (44.5 mM, 0.60 mL, 27 μmol). The reaction mixture was stirred at 80 °C for 20 h under argon. The precipitate obtained from the mixture during the reaction was collected by filtration, washed with 1,2-dichloroethane, and dried in vacco to afford *cis*-**3** as a white solid in 51.6% yield (11.0 mg). Mp: > 300 ºC. ^{1}H NMR (500 MHz, DMSO-d_6, 25 °C) δ 7.33 (d, J = 8.5 Hz, 8H, ArH), 7.19 (d, J = 2.0 Hz, 4H, ArH), 7.18 (d, J = 2.5 Hz, 4H, ArH), 7.09 (dd, J = 2.5, 8.5 Hz, 4H, ArH), 7.06 (d, J = 2.5 Hz, 4H, ArH), 6.79 (d, J = 8.5 Hz, 8H, ArH), 6.56 (d, J = 8.5 Hz, 4H, ArH), 6.27 (s, 4H, CH=CH), 1.30 (s, 36H, $C(CH_3)_3$), 1.25 (s, 36H, $C(CH_3)_3$). ^{13}C NMR (175 MHz, DMSO-d_6, 40 °C): δ 154.90, 152.16, 140.82, 140.38, 139.23, 133.79, 131.23, 130.86, 130.78, 129.00, 126.92, 125.54, 124.93, 124.34, 124.80, 120.67, 33.57, 33.52, 31.47, 31.34 (20 signals out of 21 expected ones). HRMS(ESI): m/z calcd for $[M(C_{108}H_{112}B_2Na_2O_8)–Na^+]^-$, 1581.8470; found 1581.8462.

3. Computational calculations

We used quantum chemical approaches, as implemented in the Gaussian 09 package,[21] to construct model double-stranded spiroborate helicates. Geometry optimisations were performed at different levels of theory, namely Hartree-Fock (HF) and density functional theory (DFT) using the hybrid ωB97X-D functional,[22] for dianions, monoanions and neutral helicates. For all optimised geometries, a subsequent frequency calculation was performed to verify that geometries correspond to energy minimums. The effect of basis set on geometries and properties was checked by increasing the basis set from the standard 3-21G basis up to the 6-31G*. Calculations were conducted both in vacuum and in the presence of solvent (CH_3CN) using the Polarizable Continuum Model (PCM) as implemented in Gaussian 09.

For several helicates, we have first verified at the HF/3-21G level of theory in vacuum that substitution of the ^{t}Bu groups with hydrogen atoms does not significantly change the optimized geometries and respective stability of the structures. For these simplified structures, we were able to increase the basis set up to 6-31G* and at the same time afford frequency calculations for solvated structures. In fact, relying solely on differences of electronic energies or on geometries optimized in vacuum appears to be insufficient to properly describe the relative stability of such double-stranded spiroborate helicates. In addition, geometry optimization was found to be more involved with the ωB97X-D functional than at the HF level but leads to consistent results whenever available. We thus retained the HF/6-31G* level of theory in CH_3CN and summarize the main results in Table S1. Comparison of the monoanion *cis*-$\mathbf{3_C}$ with the dianion *cis*-$\mathbf{3_E}$ and a free sodium cation needs to be corrected for basis set superposition errors (BSSE). This could be qualitatively estimated from electronic energies in vacuum where BSSE amounts to *ca*. 3 kcal mol^{-1}.

Acknowledgements

This work was supported in part by Grant-in-Aids for Scientific Research (S) from the JSPS (E.Y.) and by Program for Leading Graduate Schools "Integrative Graduate Education and Research in Green Natural Sciences", MEXT, Japan. C.K. acknowledges the HPC resources of CINES and of IDRIS under the allocations 2013-[x2013080649] made by GENCI (Grand Equipement National de Calcul Intensif) for generous support of this work. The authors are grateful to Dr. Kazuhiro Miwa (Nagoya University) and Prof. Yoshio Furusho (Kinki University) for their help in the synthesis of *trans*-**8**.

Notes and references

1 For recent reviews on molecular machines including molecular motors and artificial muscles using external stimuli, see: (*a*) V. Balzani, A. Credi, F. M. Raymo and J. F. Stoddart, *Angew. Chem., Int. Ed.*, 2000, **39**, 3348−3391; (*b*) J.-P. Collin, C. Dietrich-Buchecker, P. Gavina, M. C. Jimenez-Molero and J.-P. Sauvage, *Acc. Chem. Res.*, 2001, **34**, 477–487; (*c*) C. A. Schalley, K. Beizai and F. Vögtle, *Acc. Chem. Res.*, 2001, **34**, 465−476; (*d*) G. S. Kottas, L. L. Clarke, D. Horinek and J. Michl, *Chem. Rev.*, 2005, **105**, 1281−1376; (*e*) K. Kinbara and T. Aida, *Chem. Rev.*, 2005, **105**, 1377−1400; (*f*) V. Balzani, A. Credi, S. Silvi and M. Venturi, *Chem. Soc. Rev.*, 2006, **35**, 1135–1149; (*g*) E. R. Kay, D. A. Leigh and F. Zerbetto, *Angew. Chem., Int. Ed.*, 2007, **46**, 72–92; (*h*) V. Balzani, A. Credi and M. Venturi, *Molecular Devices and Machines: Concepts and Perspectives for the Nanoworld*, 2nd Ed., Wiley-VCH, Weinheim, 2008; (*i*) F. Niess, V. Duplan and J.-P. Sauvage, *Chem. Lett.*, 2014, **43**, 964–974; (*j*) C. J. Bruns and J. F. Stoddart, *Acc. Chem. Res.*, 2014, **47**, 2186–2199.

2 For reviews on photoresponsive molecular machines, see: (*a*) B. L. Feringa, R. A. van Delden, N. Koumura and E. M. Geertsema, *Chem. Rev.*, 2000, **100**, 1789–1816; (*b*) *Molecular Switches*, ed., B. L. Feringa, Wiley-VCH, Weinheim, 2001; (*c*) B. L. Feringa, *Acc. Chem. Res.*, 2001, **34**, 504−513; (*d*) S. Saha and J. F. Stoddart, *Chem. Soc. Rev.*, 2007, **36**, 77–92; (*e*) M.-M. Russew and S. Hecht, *Adv. Mater.*, 2010, **22**, 3348–3360; (*f*) F. D. Jochum and P. Theato, *Chem. Soc. Rev.*, 2013, **42**, 7468–7483. (*g*) C. García-Iriepa, M. Marazzi, L. M. Frutos and D. Sampedro, *RSC Adv.*, 2013, **3**, 6241–6266.

3 For leading references on photoresponsive molecular motors based on photoswitchable overcrowded C=C bonds, see: (*a*) N. Koumura, R. W. J. Zijlstra, R. A. van Delden, N. Harada and B. L. Feringa, *Nature*, 1999, **401**, 152–155; (*b*) R. A. van Delden, M. K. J. ter Wiel, M. M. Pollard, J. Vicario, N. Koumura and B. L. Feringa, *Nature*, 2005, **437**, 1337–1340; (*c*) R. Eelkema, M. M. Pollard, J. Vicario, N. Katsonis, B. S. Ramon, C. W. M. Bastiaansen, D. J. Broer and B. L. Feringa, *Nature*, 2006, **440**, 163.

4 For photoresponsive doubly threaded rotaxanes, see: (*a*) S. Tsuda, Y. Aso and T. Kaneda, *Chem. Commun.*, 2006, 3072–3074; (*b*) R. E. Dawson, S. F. Lincoln and C. J. Easton, *Chem. Commun.*, 2008, 3980–3982; (*c*) S. Li, D. Taura, A. Hashidzume, A. Harada, *Chem. Eur. J.*, 2010, **5**, 2281–2289; For a photoresponsive double helix, see: (*d*) Y. Furusho, Y. Tanaka, T. Maeda, M. Ikeda and E. Yashima, *Chem. Commun.*, 2007, 3174–3176.

5 For reviews on photoresponsive systems for molecular devices and functional materials, see: (*a*) M. Irie, *Adv. Polym. Sci.*, 1990, **94**, 27–67; (*b*) S. Kawata and Y. Kawata, *Chem. Rev.*, 2000, **100**, 1777–1788; (*c*) A. Natansohn and P. Rochon, *Chem. Rev.*, 2002, **102**, 4139–4175; (*d*) R. Klajn, J. F. Stoddart and B. A. Grzybowski, *Chem. Soc. Rev.*, 2010, **39**, 2203–2237; (*e*) R. S. Stoll and S. Hecht, *Angew. Chem., Int. Ed.*, 2010, **49**, 5054–5075.

6 H. Katagiri, T. Miyagawa, Y. Furusho and E. Yashima, *Angew. Chem., Int. Ed.*, 2006, **45**, 1741–1744.

7 (*a*) K. Miwa, Y. Furusho and E. Yashima, *Nature Chem.*, 2010, **2**, 444–449; (*b*) K. Miwa, K. Shimizu, H. Min, Y. Furusho and E. Yashima, *Tetrahedron*, 2012, **68**, 4470–4478.

8 Y. Furusho, K. Miwa, R. Asai and E. Yashima, *Chem. Eur. J.*, 2011, **17**, 13954–13957.

9 S. Yamamoto, H. Iida and E. Yashima, *Angew. Chem., Int. Ed.*, 2013, **52**, 6849–6853.

10 For examples of photoresponsive supramolecular systems using stilbene residues, see: (*a*) C. A. Stanier, S. J. Alderman, T. D. W. Claridge and H. L. Anderson, *Angew. Chem., Int. Ed.*, 2002, **41**, 1769–1772; (*b*) D.-H. Qu, Q.-C. Wang and H. Tian, *Angew. Chem., Int. Ed.*, 2005, **44**, 5296–5299; (*c*) P. Kuad, A. Miyawaki, Y. Takashima, H. Yamaguchi and A. Harada, *J. Am. Chem. Soc.*, 2007, **129**, 12630–12631; (*d*) V. Serreli, C.-F. Lee, E. R. Kay and D. A. Leigh, *Nature*, 2007, **445**, 523–527.

11 For examples of photoresponsive supramolecular systems using azobenzene residues, see: (*a*) S. Shinkai, T. Nakaji, T. Ogawa, K. Shigematsu and O. Manabe, *J. Am. Chem. Soc.*, 1981, **103**, 111–115; (*b*) H. Murakami, A. Kawabuchi, K. Kotoo, M. Kunitake and N. Nakashima, *J. Am. Chem. Soc.*, 1997, **119**, 7605–7606; (*c*) T. Muraoka, K. Kinbara, T. Aida, *Nature*, 2006, **440**, 512–515.

12 For reviews on photoresponsive synthetic polymers, polypeptides, polynucleotides, and foldamers with a single-stranded helical conformation, see: (*a*) O. Pieroni, A. Fissi and G. Popova, *Prog. Polym. Sci.*, 1998, **23**, 81–123; (*b*) E. Yashima in *Chiral Photochemistry*, ed. Y. Inoue and V. Ramamurthy, Marcel Dekker, New York, 2004, pp. 633–665; (*c*) E. Yashima, K. Maeda, H. Iida, Y. Furusho and K. Nagai, *Chem. Rev.*, 2009, **109**, 6102–6211; (*d*) Y. Kamiya and H. Asanuma, *Acc. Chem. Res.*, 2014, **47**, 1663–1672.

13 For examples of photoresponsive helical foldamers, see: (*a*) A. Khan, C. Kaiser and S. Hecht, *Angew. Chem., Int. Ed.*, 2006, **45**, 1878–1881; (*b*) C. Tie, J. C. Gallucci and J. R. Parquette, *J. Am. Chem. Soc.*, 2006, **128**, 1162–1171; (*c*) A. Khan and S. Hecht, *Chem. Eur. J.*, 2006, **12**, 4764–4774; (*d*) Y. Hua and A. H. Flood, *J. Am. Chem. Soc.*, 2010, **132**, 12838–12840; (*e*) H. Sogawa, M. Shiotsuki, H. Matsuoka and F. Sanda, *Macromolecules*, 2011, **44**, 3338–3345; (*f*) Z. Yu, S. Weidner, T. Risse and S. Hecht, *Chem. Sci.*, 2013, **4**, 4156–4167.

14 (*a*) C. L. Perrin and T. J. Dwyer, *Chem. Rev.*, 1990, **90**, 935−967; (*b*) M. Pons and O. Millet, *Prog. Nucl. Magn. Reson. Spectrosc.*, 2001, **38**, 267−324; (*c*) N. Nishimura, K. Yoza and K. Kobayashi, *J. Am. Chem. Soc.*, 2010, **132**, 777−790.

15 (*a*) D. H. Waldeck, *Chem. Rev.*, 1991, **91**, 415−436; (*b*) T. Arai and K. Tokumaru, *Chem. Rev.*, 1993, **93**, 23−39.

16 Calculation results suggest that relative Gibbs free energy between *cis*-$\mathbf{3_E}$ and *trans*-$\mathbf{3_E}$ is not significantly different (Table S1 in ESI†).

17 For photooxidation of stilbene derivatives resulting in the formation of aldehydes, see: (*a*) H. Maeda, K.-i. Nishimura, K. Mizuno, M. Yamaji, J. Oshima and S. Tobita, *J. Org. Chem.*, 2005, **70**, 9693–9701, and references therein; (*b*) M. A. Fourati, W. G. Skene, C. G. Bazuin and R. E. Prud'homme, *J. Phys. Chem. A*, 2013, **117**, 836–844.

18 C. Kabuto, S. Akine, T. Nemoto, E. Kwon, *J. Cryst. Soc. Jpn.*, 2009, **51**, 218–224.

19 D. Grebel-Koehler, D. Liu, S. De Feyter, V. Enkelmann, T. Weil, C. Engels, C. Samyn, K. Müllen, F. C. De Schryver, *Macromolecules*, 2003, **36**, 578–590.

20 F. Babudri, A. Cardone, T. Cassano, G. M. Farinola, F. Naso, R. Tommasi, *J. Organomet. Chem.*, 2008, **693**, 2631–2636.

21 M. J. Frisch, G. W. Trucks, H. B. Schlegel, G. E. Scuseria, M. A. Robb, J. R. Cheeseman, G. Scalmani, V. Barone, B. Mennucci, G. A. Petersson, H. Nakatsuji, M. Caricato, X. Li, H. P. Hratchian, A. F. Izmaylov, J. Bloino, G. Zheng, J. L. Sonnenberg, M. Hada, M. Ehara, K. Toyota, R. Fukuda, J. Hasegawa, M. Ishida, T. Nakajima, Y. Honda, O. Kitao, H. Nakai, T. Vreven, J. A. Montgomery, Jr., J. E. Peralta, F. Ogliaro, M. Bearpark, J. J. Heyd, E. Brothers, K. N. Kudin, V. N. Staroverov, R. Kobayashi, J. Normand, K. Raghavachari, A. Rendell, J. C. Burant, S. S. Iyengar, J. Tomasi, M. Cossi, N. Rega, J. M. Millam, M. Klene, J. E. Knox, J. B. Cross, V. Bakken, C. Adamo, J. Jaramillo, R. Gomperts, R. E. Stratmann, O. Yazyev, A. J. Austin, R. Cammi, C. Pomelli, J. W. Ochterski, R. L. Martin, K. Morokuma, V. G. Zakrzewski, G. A. Voth, P. Salvador, J. J. Dannenberg, S. Dapprich, A. D. Daniels, Ö. Farkas, J. B. Foresman, J. V. Ortiz, J. Cioslowski and D. J. Fox, *Gaussian 09*, *Revision A.02*, Gaussian, Inc., Wallingford CT, 2009.

22 J. D. Chai and M. Head-Gordon, *Phys. Chem. Chem. Phys.*, 2008, **10**, 6615–6620.